Spin-Direction-Spin Coupling of Quasiguided Modes in Plasmonic Crystals

Jeeban Kumar Nayak,[1,*] Harley Suchiang,[1] Subir Kumar Ray,[1] Shyamal Guchhait,[1] Ayan Banerjee,[1] Subhasish Dutta Gupta,[1,2] and Nirmalya Ghosh[1,†]

[1]*Department of Physical Sciences, Indian Institute of Science Education and Research Kolkata, Mohanpur, India, 741246*
[2]*Tata Centre for Interdisciplinary Sciences, TIFRH, Hyderabad 500107, India*

(Received 4 May 2023; accepted 25 September 2023; published 9 November 2023)

We report an unusual spin-direction-spin coupling phenomenon of light using the leaky quasiguided modes of a waveguided plasmonic crystal. This is demonstrated as simultaneous input spin-dependent directional guiding of waves (spin-direction coupling) and wave-vector–dependent spin acquisition (direction-spin coupling) of the scattered light. These effects, manifested as the forward and the inverse spin Hall effect of light in the far field, and other accompanying spin-orbit interaction effects are observed and analyzed using a momentum ($\boldsymbol{k}$) domain polarization Mueller matrix. Resonance-enabled enhancement of these effects is also demonstrated by utilizing the spectral Fano resonance of the hybridized modes. The fundamental origin and the unconventional manifestation of the spin-direction-spin coupling phenomenon from a relatively simple system, ability to probe and interpret the resulting spin-orbit phenomena in the far field through momentum-domain polarization analysis, and their regulated control in plasmonic-photonic crystals open up exciting avenues in spin-orbit-photonic research.

DOI: 10.1103/PhysRevLett.131.193803

Coupling and mutual influence of spin angular momentum (SAM), orbital angular momentum (OAM), and linear momentum of light, have led to a number of photonic spin-orbit interaction (SOI) effects in various light-matter interactions [1–14]. These have provided new insights on the universal SOI phenomena, and have opened up a new paradigm of spin-orbit photonic devices [1,2]. Among these, photonic spin-directional coupling [1–3,15,16] has attracted particular attention due to its fundamental nature and potential device applications. Such coupling is usually obtained in spatially inhomogeneous anisotropic metasurfaces through tailoring of the geometric phase gradient to break the spatial inversion symmetry [1–3,9,15]. The photonic spin-momentum locking has also been demonstrated in planar interfaces without any structures through the transverse SAM of evanescent or surface waves [1,8,16,17]. Here we report an unconventional spin-direction-spin coupling phenomenon using the leaky quasiguided modes of a one-dimensional (1D) waveguided plasmonic crystal (WPC) system. We have observed simultaneous spin-controlled directional guiding of waves and its reciprocal effect, wave-vector–dependent spin acquisition of the scattered light from the same system. While the former demonstrates the conventional spin Hall effect (SHE) in the far field, the latter is interpreted as the inverse SHE of light. The inverse SHE of light can be seen as an optical analogue of the spin injection in the solid-state spintronic devices. Here, with unpolarized light excitation (with no input SAM), the scattered light acquires specific spin polarization depending upon the direction of scattering [16,18]. Henceforth, we use the terminology "spin-direction-spin coupling" to represent the combined effect of the forward and the inverse SHE. These effects are mediated by the evolution of space-varying polarization and space-varying geometric phase due to the interaction of highly nonparaxial focused light with the polarization-anisotropic quasiguided modes of the WPC. To experimentally probe these effects in the far field, we have employed a dark-field Fourier (momentum $\boldsymbol{k}$) domain polarization Mueller matrix imaging setup. All the SOI effects are separately manifested in different characteristic $\boldsymbol{k}$ domain Mueller matrix elements, enabling their unique interpretation and quantification in a single experimental embodiment [2]. The highly sought after controlled enhancement of the SOI effects is also demonstrated by utilizing the Fano-type resonances of the hybridized modes of the WPC system [1,6,10,19].

Our custom-designed dark-field polarization microscopic arrangement is capable of recording the complete spectral and spatially resolved polarization response of a sample [20,21] [Fig. 1(a)]. This system employs broadband white light for excitation, and records polarization-resolved images of the sample-scattered light at any selected wavelength between $\lambda = 400$–725 nm. The 4×4 Mueller matrix is constructed utilizing thirty-six polarization-resolved intensity measurements by sequentially generating and analyzing six different linear and circular polarization states (see Supplemental Material for details [22,27]). The spectral and the Fourier domain Mueller matrix images (distributions of transverse momenta, $k_\perp$: k_x, k_y) are recorded at different selected wavelengths to observe and interpret the different SOI effects.

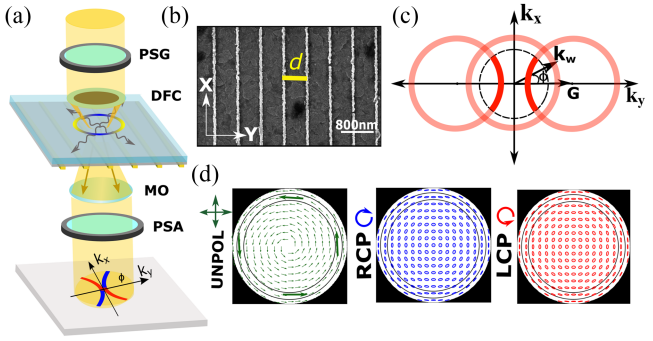

FIG. 1. (a) Schematic of the dark-field Fourier domain Mueller matrix microscopy system. PSG and PSA: polarization state generator and analyzer units, DFC: dark-field condenser, MO: microscope objective. (b) Typical SEM images of the WPC. (c) Formation of ringlike intensity distribution corresponding to the quasiguided modes in the $\boldsymbol{k}$ domain, and detection of arc segments of the k contours are illustrated. Radii of the diffraction rings are decided by the wave vector of the quasiguided modes $|\boldsymbol{k}_w|$. The Grating vector is defined as $\boldsymbol{G} = 2\pi/d$. (d) Theoretically simulated azimuthally varying polarization distribution of the focused light at the sample site for incident unpolarized, right (RCP), and left (LCP) circular polarized light. Marked annular region corresponds to the NA of the dark-field condenser $(0.8 - 0.92)$.

The WPC sample comprises of periodic gold (Au) grating on top of an indium tin oxide (ITO) waveguiding layer (thickness ≈190 nm), which is deposited on a glass substrate [Fig. 1(b)]. The WPC has been the subject of extensive recent research due to its unique ability to couple and control both the electronic and photonic resonances [21,28–30]. The highly confined fields of the hybridized modes in such a system is expected to bring forth interesting SOI effects [31], which is investigated here. The geometrical parameters of the WPC are chosen with the aim to obtain strong spectral overlap between the narrow waveguide modes and the broad surface plasmon resonance modes within the desired spectral range ($\lambda \approx 460$–580 nm) [21]. For this purpose, the WPC is simulated using the finite element method [32], and the optimized WPC is fabricated using electron-beam lithography (see Supplemental Material for details [22]). The optimized grating parameters are periodicity ≈550 nm, width ≈90 nm, and thickness ≈20 nm.

For incident transverse magnetic (TM-$\boldsymbol{y}$) polarization [shown in Fig. 1(b)], the near-field hybridization takes place between the TM waveguide modes excited in the ITO layer and the surface plasmon resonances of the Au gratings. On the other hand, with transverse electric (TE-$\boldsymbol{x}$) polarization excitation, near-field interference occurs between the TE waveguide modes with the incident photon continuum. In either case, these couplings are manifested in the far-field radiation as spectrally asymmetric Fano resonances [21,28]. Importantly, the different amplitude and phase distributions of the hybridized modes for TM and TE polarizations lead to the exhibition of strong amplitude anisotropy (quantified by linear diattenuation d_{WPC}, differential attenuation of orthogonal linear polarizations) and phase anisotropy (linear retardance δ_{WPC}, phase difference between orthogonal linear polarizations) effects in the Fano resonance spectra [21] (see Supplemental Material for details [22]). Owing to the presence of the Au grating, the hybridized waveguide modes become leaky [28] and the leakage radiation is collected by a microscope objective to obtain both the polarization resolved Fourier domain images, and the scattering spectra. These quasiguided modes get localized as arclike diffraction patterns in the Fourier plane (see Supplemental Material for details [22]). The high numerical aperture (NA) dark-field condenser in our illumination geometry ensures excitation of both the waveguide and the plasmonic modes of the WPC. The ITO waveguide, (which is an isotropic homogeneous medium) taken separately, will lead to circular isocontours in the $\boldsymbol{k}$ space ($k_\perp = k_w$), as the waveguide modes are excited in all possible directions due to high NA illumination. Analogous diffracted circular contours can be observed for the plasmonic guide with the grating coupler also [33,34]. However, due to the hybridization and the broken symmetry of the coupled guided modes in the WPC system, the Fourier domain intensity patterns may reflect elliptical or a more complicated shape of the k contours. In Fig. 1(c), we illustrate how the grating coupling helps in recording the $\boldsymbol{k}$ space arc segments of the quasiguided modes using our collection objective (NA shown by dotted line). The circular shapes of the rings are used for simplified illustration purpose only. We could record arc segments of the $+1$ and -1 orders of the diffraction patterns only, as the spatial frequency ($\boldsymbol{k}$) is limited by the NA (NA ≈ 0.8) of the objective ($|\boldsymbol{k}| \leq k_0 \times \mathrm{NA}$) [Fig. 1(c)]. The SOI effects are manifested in the polarization-resolved intensities of these $\boldsymbol{k}$ domain arc segments. Note that the high NA focusing of the dark-field condenser generates space (azimuthally) varying inhomogeneous polarization at the sample plane [shown in Fig. 1(d)], which is at the heart of all the SOI effects, described subsequently.

The spin to orbital AM coupling in symmetric cases for nonparaxial propagation of polarized light (e.g., in tight focusing, imaging and scattering [35,36]) can be described by azimuthal (ϕ) rotational transformation of the three-dimensional electric fields corresponding to different wave vectors ($\boldsymbol{k}$). This yields a 3×3 momentum ($\boldsymbol{k}$) domain Jones matrix with azimuthal orientation [1] (see Supplemental Material for details [22]). The SOIs exhibited in the cylindrically symmetric spatially inhomogeneous anisotropic medium (having azimuthal orientation of the anisotropy axis) can also be described using the 2×2 block corresponding to the transverse field components of this Jones matrix. SOIs in these scenarios are mediated by the azimuthally varying geometric phase, which evolves either due to azimuthal trajectory of the polarized field (spin

redirection Berry phase) or due to azimuthal anisotropy axis orientation (Pancharatnam phase). The experimentally measurable $\boldsymbol{k}$ domain 4×4 Mueller matrix corresponding to the 2×2 Jones matrix, contains all the necessary information. This exhibits the characteristic form of a linear diattenuating (partially polarizing) retarder (wave plate) with azimuthal orientation [36] (see Supplemental Material for details [22]). Here, however, there is a composite effect, which can be modeled by the sequential product of two Mueller matrices of two successive polarization transforming events: (i) generation of spatially varying polarization due to tight focusing, which is a geometric effect described by the Mueller matrix of a linear diattenuating retarder with azimuthal (ϕ) orientation $M_f(d_f, \delta_f, \phi)$ having linear diattenuation (d_f) and linear retardance (δ_f); (ii) followed by its interaction with the anisotropic WPC system, described by the Mueller matrix of a linear diattenuating retarder with fixed orientation axis as determined by the axis of the Au grating M_{WPC} $(d_{\mathrm{WPC}}, \delta_{\mathrm{WPC}}, \phi = 0)$.

We experimentally recorded both the 1×4 Stokes vectors ($\boldsymbol{S}$) of the leakage radiation from the quasiguided modes for selected input polarization states, and the full 4×4 Mueller matrix of the WPC in the $\boldsymbol{k}$ domain. The "four-lobe" azimuthal intensity patterns $(\propto \cos 2\phi, \sin 2\phi)$ in the $\boldsymbol{k}$ space arc segments of the second ($\boldsymbol{S_1}$) and the third ($\boldsymbol{S_2}$) Stokes vector elements with input circularly polarized light [Fig. 2(a)] demonstrates well-known signatures of SAM to intrinsic-OAM conversion through the evolution of azimuthal geometric phase [37,38] (see Supplemental Material for details [22]). Similar signatures are also evident in the fourth Stokes vector element ($\boldsymbol{S_3}$) with input horizontal and vertical polarizations [Fig. 2(b)]. These results are shown for the wavelength $\lambda = 440$ nm ($\Delta\lambda \approx 40$ nm), which is purposely selected away from the central wavelength region of the Fano resonance (shown subsequently). The $\boldsymbol{k}$ domain Mueller matrix [Fig. 2(c)] partly resembles SOI features of a linear diattenuating retarder having azimuthal orientation of anisotropy axis [36] (see Supplemental Material for details). While the azimuthal intensity lobes of the $M_{24/42}$, $M_{34/43}$ elements carry the signature of SAM to intrinsic OAM conversion due to an azimuthal (vortex) linear retarder, $M_{12/21}$ and $M_{13/31}$ represent similar SOI effects due to a vortex linear diattenuator [38]. The azimuthal intensity patterns in the $M_{23/32}$ elements provide evidence of the evolution of azimuthal geometric phase, as these elements record signatures correspond to the rotation of linear polarization. The $(\propto \cos 2\phi, \sin 2\phi)$ intensity lobes imply an accumulation of the 4π phase for a full 2π azimuthal rotation in the $\boldsymbol{k}$ space corresponding to the emergence of phase singularity with a topological charge of ± 2 for opposite circular polarizations. Surprisingly, the $\boldsymbol{k}$ domain Mueller matrix additionally exhibits nonzero magnitudes of the circular anisotropy descriptor M_{14} and M_{41}

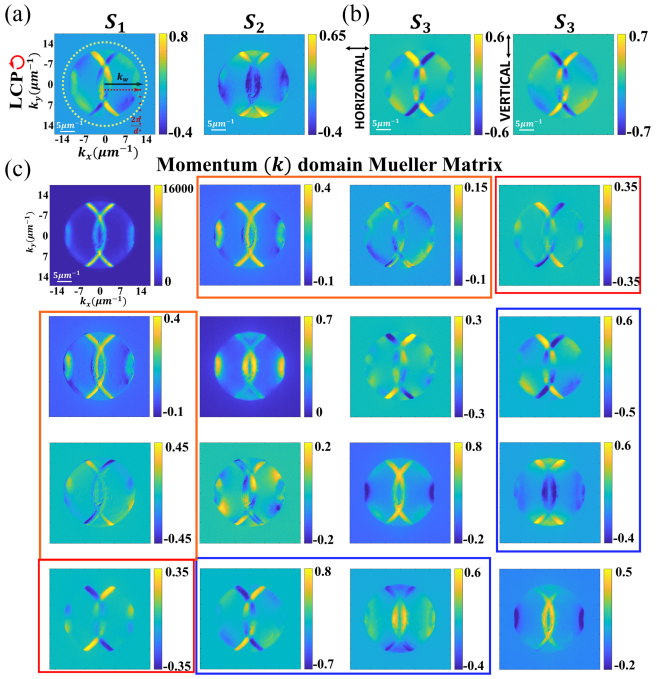

FIG. 2. Experimental Stokes vector elements of the leakage light from the quasiguided modes corresponding to the $\boldsymbol{k}$-domain arc segments, (a) $\boldsymbol{S_1}$ and $\boldsymbol{S_2}$ elements with input LCP and RCP, (b) $\boldsymbol{S_3}$ with input horizontally and vertically polarized light. (c) The $\boldsymbol{k}$ domain 4×4 Mueller matrix of the WPC. Signature of the vortex linear diattenuator (elements marked by orange boxes), vortex linear retarder (blue boxes), and the elements M_{14} and M_{41} describing the SHE (red boxes) are highlighted. In this figure (a) and in subsequent figures, the following parameters are displayed: boundaries of the Brillouin zone($2\pi/d$) (brown dotted line); wave vector of the quasiguided modes ($\boldsymbol{k_w}$) (black solid line); light line ($2\pi/\lambda$) (yellow dotted circle); and scale bar in the $\boldsymbol{k}$ space (white solid lines).

elements, which cannot be explained using the conventional polarization matrix of SOI [1,36]. We identify these as exclusive signatures of forward and inverse SHE of light in the far field. These experimentally observed SOI effects were further confirmed by theoretically generating Mueller matrices analogous to the experimental ones (see Supplemental Material for details [22]).

The forward SHE is usually manifested as incident spin (circular polarization)-dependent shifting of the trajectory of light [1,3,39]. This can be probed by measuring the difference in the distributions of the total scattered intensities for input RCP and LCP light ($\mathrm{RI_{total}} - \mathrm{LI_{total}}$), which determines the circular diattenuation-descriptor M_{14} Mueller matrix element. Here, this is manifested as input circular polarization-dependent "lighting-up" of azimuthal (ϕ) intensity lobes along orthogonal radial directions in the $\boldsymbol{k}$ space arc segments [Fig. 3(a)]. With input unpolarized light (U), azimuthal intensity lobes along orthogonal radial directions are observed while postselecting the RCP and LCP components of the scattered light [Fig. 3(b)]. This is

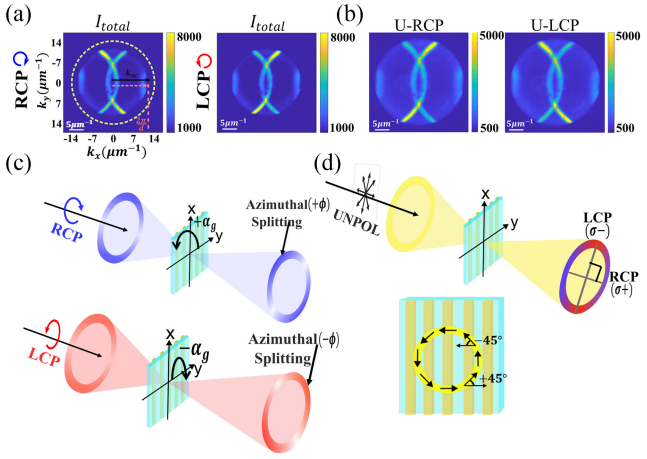

FIG. 3. (a) Input circular polarization-dependent azimuthal (ϕ) intensity lobes along orthogonal radial directions are observed in the total detected intensities in the $\boldsymbol{k}$ space with input RCP and LCP states: forward SHE. (b) Inverse SHE is demonstrated as the formation of flipped azimuthal lobes while postselecting the RCP and LCP components of the scattered light for unpolarized (U) excitation (U-RCP and U-LCP). (c) Forward SHE: azimuthal splitting of intensity lobes for LCP and RCP inputs due to opposite azimuthal gradients of geometric phase. (d) Inverse SHE: for unpolarized input, the generated azimuthally varying polarization at the WPC plane imparts opposite elliptical polarizations at different azimuthal angles ($\pm\phi$).

interpreted as the inverse SHE of light, which is encoded in the M_{41} element that describes the circular polarizance effect (see Supplemental Material for details [22]).

Using sequential products of two Mueller matrices, expressions for the forward(M_{14}) and inverse(M_{41}) SHE-descriptor Mueller matrix elements can be obtained as (see Supplemental Material for details [22]).

$$M_{14} = -d_{\mathrm{WPC}}\sqrt{1-d_f^2}\,\sin(\delta_f)\,\sin(2\phi)$$
$$M_{41} = d_f\sqrt{1-d_{\mathrm{WPC}}^2}\,\sin(\delta_{\mathrm{WPC}})\,\sin(2\phi). \qquad (1)$$

Clearly, nonzero magnitudes of both these elements arise when all the linear anisotropy parameters are nonzero ($d_f, d_{\mathrm{WPC}} \neq 0$ and $\delta_f, \delta_{\mathrm{WPC}} \neq 0$). While $d_f \neq 0$ due to focusing is a geometric effect [36], the WPC exhibits intrinsic d_{WPC} and δ_{WPC} effects due to the amplitude and phase differences between the leakage radiation from the quasiguided modes excited by orthogonal (y-x) linear polarizations [21]. As discussed before, with input unpolarized light, the high NA focusing generates an azimuthally varying linear polarization at the WPC [Fig. 1(d)]. This consequently imparts opposite circular (elliptical) polarizations to the leakage radiation at opposite azimuthal angles ($\pm\phi$) with respect to the axis of the grating [Fig. 3(d), results shown in Fig. 3(b)]. This inverse SHE can be interpreted as a $\boldsymbol{k}$ domain geometric circular or elliptical polarizer comprising of an azimuthal linear polarizer (due to the focusing transformation) followed by a wave plate (linear retardance of the WPC). The forward SHE can be interpreted as a $\boldsymbol{k}$ domain "geometric circular or elliptical analyzer" that allows selective leakage of radiation from the quasiguided modes along orthogonal radial directions for input RCP and LCP states. This can be understood from the opposite azimuthal gradient of geometric phase ($\pm\phi$) obtained for input RCP and LCP states [Fig. 3(c)]. Since the direction of the leakage radiation is determined by the wave vector ($\boldsymbol{k_w}$) of the quasiguided modes, [34] and the $\boldsymbol{k}$ domain intensity patterns carry exclusive information on this, the observed effects are clearly far-field manifestations of the spin-coupled excitation of the quasiguided modes along orthogonal radial directions (see Supplemental Material for details [22]). The origin and manifestations of these are thus distinctly different from the usual spin-momentum locking phenomena [1,2,8,16].

As evident from Eq. (1), the amplitude anisotropy (d_{WPC}) and the phase anisotropy (δ_{WPC}) parameters of the WPC determines the strength of the forward and the inverse SHEs. As discussed previously, the different near-field spatial distributions and strength of the hybridized modes of the WPC for orthogonal TM and TE linear polarizations lead to strongly anisotropic Fano resonances in the far field (see Supplemental Material for details [22]), manifesting as strongly enhanced d_{WPC} and δ_{WPC} anisotropy parameters. This can thus be exploited for controlled enhancement of the SHEs and the other SOI effects, as demonstrated in Fig. 4. Prominent spectrally asymmetric Fano resonances ($\lambda \approx 460$–580 nm, with a Fano dip around $\lambda =$ 490–500 nm) for both the TM and TE polarizations [Fig. 4(a)], provide evidence of the mode hybridization in the WPC. The inherent dissipation losses associated with

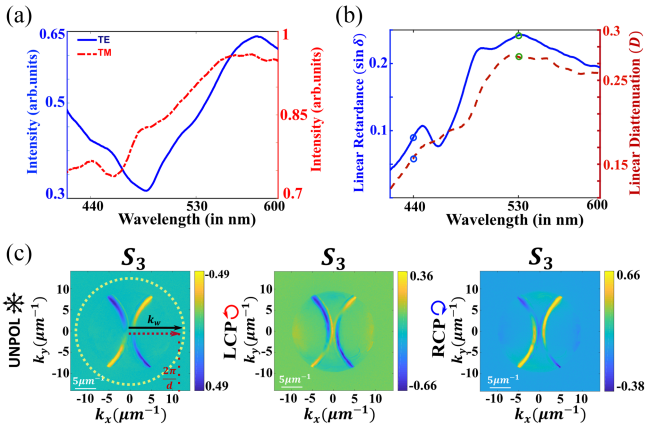

FIG. 4. (a) Scattering spectra from the leaky quasiguided modes of the WPC for TM (red dotted line) and TE (solid blue line) polarization excitation. (b) Spectral variation of the linear retardance (solid blue line) and linear diattenuation (brown dashed line) demonstrates enhancement of these anisotropy parameters around the Fano resonance wavelengths. (c) Stokes vector element $\boldsymbol{S_3}$ of the $\boldsymbol{k}$ space arc segments with input unpolarized (U), LCP and RCP light at $\lambda = 530$ nm.

the Au grating, is however, evident from the relatively broader line shape of Fano resonances (see Supplemental Material for details [22–26]). Importantly, sharp increase of the Mueller matrix-derived d_{WPC} and δ_{WPC} parameters around the Fano spectral asymmetry region [Fig. 4(b)] provides clear evidence for the polarization-anisotropic nature of the hybridization of the quasiguided modes and resulting enhancement of the anisotropy parameters [10,21]. Consequently, Fano resonance-enabled enhancement of the inverse SHE and spin to orbital AM conversion [Fig. 4(c)] are accordingly observed in the azimuthal lobes in the Stokes vector $\boldsymbol{S_3}$ corresponding to the $\boldsymbol{k}$ space arc segments for $\lambda = 530$ nm, which falls within the central Fano asymmetry region. The enhancement can be clearly seen in the magnitude of $\boldsymbol{S_3}$ for input unpolarized, LCP and RCP states at $\lambda = 530$ nm as compared to $\lambda = 440$ nm (see Supplemental Material for details [22]), which is spectrally away from the Fano resonance.

In conclusion, we have observed an unconventional "spin-direction-spin coupling phenomenon" in a simple system of a waveguided plasmonic crystal having no structural anisotropy gradient, which manifested as simultaneous forward and inverse SHE of light in the far field. A momentum domain polarization Mueller matrix setup is utilized to decouple, probe, and quantify these effects and a plethora of other accompanying SOI effects. These unusual SOI phenomena draw their origin from spatially varying polarization of highly nonparaxial tightly focused light, and its interaction with the polarization-anisotropic quasiguided modes. This opens up interesting avenues by exploiting spatially tailored polarization inhomogeneity in relatively simple metasurfaces and this also paves the way for the use of unpolarized light in spin-orbit photonic research. The demonstrated enhancement and tunability of multiple SOI effects in the same nanophotonic system using the hybridized plasmonic and photonic resonances, bodes well for future multifunctional spin-photonic nanodevice applications. For example, forward and inverse SHE in the WPC can be used for input spin(polarization)-controlled directional guiding or switching of light, and for the processing of polarization-encoded information, polarization sorting etc. at nanometer length scale. The momentum domain Mueller matrix microscopy using leakage radiation introduced in this study also holds considerable promise as a unique experimental tool for studying a broad variety of spin-polarization optical phenomena in diverse nano-optical systems, which may also be explored for sensing applications [33].

*jkn19rs027@iiserkol.ac.in
†nghosh@iiserkol.ac.in

[1] K. Y. Bliokh, F. J. Rodríguez-Fortuño, F. Nori, and A. V. Zayats, Spin–orbit interactions of light, Nat. Photonics **9**, 796 (2015).
[2] T. Cui, L. Sun, B. Bai, and H.-B. Sun, Probing and imaging photonic spin-orbit interactions in nanostructures, Laser Photonics Rev. **15**, 2100011 (2021).
[3] X. Yin, Z. Ye, J. Rho, Y. Wang, and X. Zhang, Photonic spin Hall effect at metasurfaces, Science **339**, 1405 (2013).
[4] K. Y. Bliokh, D. Smirnova, and F. Nori, Quantum spin Hall effect of light, Science **348**, 1448 (2015).
[5] K. Y. Bliokh, I. V. Shadrivov, and Y. S. Kivshar, Goos–hänchen and Imbert–Fedorov shifts of polarized vortex beams, Opt. Lett. **34**, 389 (2009).
[6] D. Lin, P. Fan, E. Hasman, and M. L. Brongersma, Dielectric gradient metasurface optical elements, Science **345**, 298 (2014).
[7] A. Aiello, P. Banzer, M. Neugebauer, and G. Leuchs, From transverse angular momentum to photonic wheels, Nat. Photonics **9**, 789 (2015).
[8] F. J. Rodríguez-Fortuño, G. Marino, P. Ginzburg, D. O'Connor, A. Martínez, G. A. Wurtz, and A. V. Zayats, Near-field interference for the unidirectional excitation of electromagnetic guided modes, Science **340**, 328 (2013).
[9] N. Shitrit, I. Yulevich, E. Maguid, D. Ozeri, D. Veksler, V. Kleiner, and E. Hasman, Spin-optical metamaterial route to spin-controlled photonics, Science **340**, 724 (2013).
[10] E. Karimi, S. A. Schulz, I. De Leon, H. Qassim, J. Upham, and R. W. Boyd, Generating optical orbital angular momentum at visible wavelengths using a plasmonic metasurface, Light Sci. Appl. **3**, e167 (2014).
[11] W. Liu, B. Wang, Y. Zhang, J. Wang, M. Zhao, F. Guan, X. Liu, L. Shi, and J. Zi, Circularly polarized states spawning from bound states in the continuum, Phys. Rev. Lett. **123**, 116104 (2019).
[12] M. Mazanov, O. Yermakov, A. Bogdanov, and A. Lavrinenko, On anomalous optical beam shifts at near-normal incidence, APL Photonics **7** (2022).
[13] X. Ling, F. Guan, X. Cai, S. Ma, H.-X. Xu, Q. He, S. Xiao, and L. Zhou, Topology-induced phase transitions in spin-orbit photonics, Laser Photonics Rev. **15**, 2000492 (2021).
[14] J. Wang, L. Shi, and J. Zi, Spin Hall effect of light via momentum-space topological vortices around bound states in the continuum, Phys. Rev. Lett. **129**, 236101 (2022).
[15] W. Zhu, H. Zheng, Y. Zhong, J. Yu, and Z. Chen, Wave-vector-varying pancharatnam-berry phase photonic spin Hall effect, Phys. Rev. Lett. **126**, 083901 (2021).
[16] D. O'connor, P. Ginzburg, F. J. Rodríguez-Fortuño, G. A. Wurtz, and A. V. Zayats, Spin–orbit coupling in surface plasmon scattering by nanostructures, Nat. Commun. **5**, 5327 (2014).
[17] K. Y. Bliokh, A. Y. Bekshaev, and F. Nori, Extraordinary momentum and spin in evanescent waves, Nat. Commun. **5**, 3300 (2014).
[18] R. Fiederling, M. Keim, G. a. Reuscher, W. Ossau, G. Schmidt, A. Waag, and L. Molenkamp, Injection and detection of a spin-polarized current in a light-emitting diode, Nature (London) **402**, 787 (1999).
[19] N. Yu, P. Genevet, M. A. Kats, F. Aieta, J.-P. Tetienne, F. Capasso, and Z. Gaburro, Light propagation with phase discontinuities: Generalized laws of reflection and refraction, Science **334**, 333 (2011).
[20] S. Bhunia, S. Chandel, S. K. Karan, S. Dey, A. Tiwari, S. Das, N. Kumar, R. Chowdhury, S. Mondal, I. Ghosh *et al.*, Autonomous self-repair in piezoelectric molecular crystals, Science **373**, 321 (2021).

[21] S. K. Ray, S. Chandel, A. K. Singh, A. Kumar, A. Mandal, S. Misra, P. Mitra, and N. Ghosh, Polarization-tailored Fano interference in plasmonic crystals: A Mueller matrix model of anisotropic Fano resonance, ACS Nano **11**, 1641 (2017).
[22] See Supplemental Material at http://link.aps.org/supplemental/10.1103/PhysRevLett.131.193803 for detailed theoretical analysis and spectral responses of the waveguided plasmonic crystal, which includes Refs. [23–26].
[23] S. V. Boriskina, T. A. Cooper, L. Zeng, G. Ni, J. K. Tong, Y. Tsurimaki, Y. Huang, L. Meroueh, G. Mahan, and G. Chen, Losses in plasmonics: From mitigating energy dissipation to embracing loss-enabled functionalities, Adv. Opt. Photonics **9**, 775 (2017).
[24] G. Sun, L. Yuan, Y. Zhang, X. Zhang, and Y. Zhu, Q-factor enhancement of Fano resonance in all-dielectric metasurfaces by modulating meta-atom interactions, Sci. Rep. **7**, 8128 (2017).
[25] S. Linden, J. Kuhl, and H. Giessen, Controlling the interaction between light and gold nanoparticles: Selective suppression of extinction, Phys. Rev. Lett. **86**, 4688 (2001).
[26] A. Christ, S. G. Tikhodeev, N. A. Gippius, J. Kuhl, and H. Giessen, Waveguide-plasmon polaritons: Strong coupling of photonic and electronic resonances in a metallic photonic crystal slab, Phys. Rev. Lett. **91**, 183901 (2003).
[27] J. S. Baba, J.-R. Chung, A. H. DeLaughter, B. D. Cameron, and G. L. Cote, Development and calibration of an automated mueller matrix polarization imaging system, J. Biomed. Opt. **7**, 341 (2002).
[28] A. Christ, T. Zentgraf, J. Kuhl, S. G. Tikhodeev, N. A. Gippius, and H. Giessen, Optical properties of planar metallic photonic crystal structures: Experiment and theory, Phys. Rev. B **70**, 125113 (2004).
[29] J. K. Nayak, S. Guchhait, A. K. Singh, and N. Ghosh, Role of avoided crossing and weak value amplification on enhanced Faraday effect in magnetoplasmonic systems, Commun. Phys. **4**, 1 (2021).
[30] M. F. Limonov, M. V. Rybin, A. N. Poddubny, and Y. S. Kivshar, Fano resonances in photonics, Nat. Photonics **11**, 543 (2017).
[31] U. Stella, T. Grosjean, N. De Leo, L. Boarino, P. Munzert, J. R. Lakowicz, and E. Descrovi, Vortex beam generation by spin-orbit interaction with Bloch surface waves, ACS Photonics **7**, 774 (2020).
[32] J. M. McMahon, A.-I. Henry, K. L. Wustholz, M. J. Natan, R. G. Freeman, R. P. Van Duyne, and G. C. Schatz, Gold nanoparticle dimer plasmonics: Finite element method calculations of the electromagnetic enhancement to surface-enhanced Raman spectroscopy, Anal. Bioanal. Chem. **394**, 1819 (2009).
[33] P. Kvasnička and J. Homola, Convenient method of micrometer-scale excitation of propagating surface plasmons by a focused laser beam, Plasmonics **9**, 737 (2014).
[34] R. Lopez-Boada, C. J. Regan, D. Dominguez, A. A. Bernussi, and L. G. De Peralta, Fundaments of optical far-field subwavelength resolution based on illumination with surface waves, Opt. Express **21**, 11928 (2013).
[35] B. Richards and E. Wolf, Electromagnetic diffraction in optical systems, ii. structure of the image field in an aplanatic system, Proc. R. Soc. A **253**, 358 (1959).
[36] S. D. Gupta, N. Ghosh, and A. Banerjee, *Wave Optics: Basic Concepts and Contemporary Trends* (CRC Press, Boca Raton, 2015).
[37] O. G. Rodríguez-Herrera, D. Lara, K. Y. Bliokh, E. A. Ostrovskaya, and C. Dainty, Optical nanoprobing via spin-orbit interaction of light, Phys. Rev. Lett. **104**, 253601 (2010).
[38] J. Soni, S. Ghosh, S. Mansha, A. Kumar, S. D. Gupta, A. Banerjee, and N. Ghosh, Enhancing spin-orbit interaction of light by plasmonic nanostructures, Opt. Lett. **38**, 1748 (2013).
[39] Y. Liu, X. Ling, X. Yi, X. Zhou, S. Chen, Y. Ke, H. Luo, and S. Wen, Photonic spin Hall effect in dielectric metasurfaces with rotational symmetry breaking, Opt. Lett. **40**, 756 (2015).